Geochemistry Geophysics Geosystems G3

Article
Volume 11
2 September 2010
Q0AA10, doi:10.1029/2010GC003084
ISSN: 1525-2027

Published by AGU and the Geochemical Society

A geologically constrained Monte Carlo approach to modeling exposure ages from profiles of cosmogenic nuclides: An example from Lees Ferry, Arizona

Alan J. Hidy and John C. Gosse
Department of Earth Sciences, Dalhousie University, Halifax, Nova Scotia B3H 4R2, Canada (alanhidy@dal.ca; john.gosse@dal.ca)

Joel L. Pederson
Department of Geology, Utah State University, Logan, Utah 84322-4505, USA (joel.pederson@usu.edu)

Jann Paul Mattern
Department of Mathematics and Statistics, Dalhousie University, Halifax, Nova Scotia B3H 3J5, Canada (paul.mattern@dal.ca)

Robert C. Finkel
Earth and Planetary Science Department, University of California, 371 McCone Hall, Berkeley, California 94720-4767, USA (rfinkel@berkeley.edu)

Also at CEREGE, BP 80, Europole Méditerranéen de l'Arbois, F-13545 Aix en Provence CEDEX 4, France

[1] We present a user-friendly and versatile Monte Carlo simulator for modeling profiles of in situ terrestrial cosmogenic nuclides (TCNs). Our program (available online at http://geochronology.earthsciences.dal.ca/downloads-models.html) permits the incorporation of site-specific geologic knowledge to calculate most probable values for exposure age, erosion rate, and inherited nuclide concentration while providing a rigorous treatment of their uncertainties. The simulator is demonstrated with ^{10}Be data from a fluvial terrace at Lees Ferry, Arizona. Interpreted constraints on erosion, based on local soil properties and terrace morphology, yield a most probable exposure age and inheritance of $83.9^{+19.1}_{-14.1}$ ka, and $9.49^{+1.21}_{-2.52} \times 10^4$ atoms g^{-1}, respectively (2σ). Without the ability to apply some constraint to either erosion rate or age, shallow depth profiles of any cosmogenic nuclide (except for nuclides produced via thermal and epithermal neutron capture, e.g., ^{36}Cl) cannot be optimized to resolve either parameter. Contrasting simulations of ^{10}Be data from both sand- and pebble-sized clasts within the same deposit indicate grain size can significantly affect the ability to model ages with TCN depth profiles and, when possible, sand—not pebbles—should be used for depth profile exposure dating.

Components: 9500 words, 7 figures, 4 tables.

Keywords: ^{10}Be; desert pavement; TCN; Grand Canyon; alluvial fan; active tectonics.

Index Terms: 1150 Geochronology: Cosmogenic-nuclide exposure dating (4918); 1105 Geochronology: Quaternary geochronology; 8175 Tectonophysics: Tectonics and landscape evolution.

Received 17 February 2010; **Accepted** 29 June 2010; **Published** 2 September 2010.

Hidy, A. J., J. C. Gosse, J. L. Pederson, J. P. Mattern, and R. C. Finkel (2010), A geologically constrained Monte Carlo approach to modeling exposure ages from profiles of cosmogenic nuclides: An example from Lees Ferry, Arizona, *Geochem. Geophys. Geosyst.*, *11*, Q0AA10, doi:10.1029/2010GC003084.

Theme: EarthTime: Advances in Geochronological Technique
Guest Editors: D. Condon, G. Gehrels, M. Heizler, and F. Hilgen

1. Introduction

[2] Analyses of the distribution with depth of concentrations of TCNs in amalgamated sediment samples—"depth profiles"—are useful for simultaneously determining exposure ages, rates of erosion or aggradation, and inherited TCN concentrations in a variety of geomorphic settings [*Anderson et al.*, 1996]. Recently, it has been demonstrated that depth profiles of ^{10}Be where TCN concentrations are not yet in equilibrium with the landscape will converge to a unique solution of exposure age, erosion rate, and inheritance when accounting for both nucleogenic and muogenic production pathways [*Braucher et al.*, 2009]. Previous depth profile approaches used χ^2 minimization or Monte Carlo methods [e.g., *Anderson et al.*, 1996; *Phillips et al.*, 1998; *Stone et al.*, 1998; *Brocard et al.*, 2003; *Matsushi et al.*, 2006; *Riihimaki et al.*, 2006; *Braucher et al.*, 2009], but provided limited integration of age-inheritance-erosion rate solutions and an explicit treatment of error.

[3] Driven by recent rejuvenation in active tectonics and surface processes research, there is an increasing need for a TCN depth-profile analysis tool that provides solutions of erosion rate, inheritance and TCN inventories of catchments, and surface exposure ages in unconsolidated sediment with physical estimates of uncertainties in these variables. Here, we introduce a versatile, user-friendly, and widely applicable depth-profile simulator designed both in MathCad™ and Matlab™ for modeling profiles of cosmogenic nuclides that: 1) incorporates geologic knowledge about the study area and soils, 2) explicitly and dynamically propagates error from all pertinent internal sources, 3) yields not just optimized values for exposure age, rate of erosion, and inheritance, but most probable values for each parameter from parameter space distributions that fully incorporate user-defined and inferred error, 4) is easy to use and time efficient so that profile data can be rapidly analyzed without specialist consultation, and 5) is freely available for download. The model is currently available for ^{10}Be and ^{26}Al, but is also appropriate for ^{14}C, and ^{21}Ne. A different model will soon be available for thermal and epithermal neutron produced TCN. We demonstrate the utility of the geologically constrained Monte Carlo approach using cosmogenic ^{10}Be depth profiles to determine the age (and explicit uncertainty of that age) of the deposition of an alluvial terrace deposit at Lees Ferry, Arizona.

2. Background

2.1. Why Use a Depth Profile?

[4] To exposure date Late Cenozoic sediments within landforms—such as alluvial fans, fluvial and marine terraces, marine and lacustrine beaches, and raised deltas—one must consider the possible effects of erosion and aggradation, as well as a number of other controls on TCN concentration [*Gosse and Phillips*, 2001]. For example, the sediment may have been previously exposed, or mixed by bioturbation, cryoturbation, or pedogenesis, or the bulk density of the sediment may have varied with time due to pedogenesis or changes in water content. For sediments that have not been vertically mixed, a depth profile can be utilized to account for a change in TCN production rate as secondary cosmic ray flux attenuates through the material. For nuclides that are produced only from high energy nuclear and muogenic reactions (e.g., ^{10}Be, ^{14}C, ^{26}Al, and ^{21}Ne), the concentration C (atoms g^{-1}) for a specific nuclide m as a function of depth z (cm), exposure time t (a), and erosion rate ε (cm a^{-1}) can be written as

$$C_m(z,\varepsilon,t) = \sum_i \frac{P(0)_{m,i}}{\left(\frac{\varepsilon\rho_z}{\Lambda_i}+\lambda_m\right)} \cdot \exp\left(-\frac{z\rho_z}{\Lambda_i}\right) \cdot \left[1-\exp\left(-t\left(\frac{\varepsilon\rho_z}{\Lambda_i}+\lambda_m\right)\right)\right] + C_{inh,m}\cdot\exp(-\lambda_m t) \quad (1)$$

where i represents the various production pathways for nuclide m (neutron spallation, fast muon spallation, and negative muon capture), $P(0)_{m,i}$ is the site-specific surface production rate for nuclide m via production pathway i (atoms g^{-1} a^{-1}), λ_m is the

decay constant for radionuclide m (a^{-1}), ρ_z is the cumulative bulk density at depth z (g cm^{-3}), Λ_i is the attenuation length of production pathway i (g cm^{-2}), and $C_{inh,m}$ is the inherited (depositional) concentration of nuclide m (atoms g^{-1} a^{-1}). Although theoretical production from muons does not behave as a simple exponential function with depth as described by equation (1) [*Heisinger et al.*, 2002a, 2002b], it has been shown that reasonable approximations to muon production can be made with multiple exponential terms for muon production pathways [e.g., *Granger and Smith*, 2000; *Schaller et al.*, 2002]. In this depth profile simulator, five exponential terms in accordance with equation (1) are used to approximate the total muon production with depth —two terms for fast muon spallation, and three terms for negative muon capture.

[5] Curves generated from equation (1) decrease with depth as the sum of exponentials to an asymptote that identifies the inheritance of the profile. Inheritance is the TCN concentration that existed in the sample prior to final deposition, i.e., it is the concentration accumulated during exposure on a hillslope, during temporary sediment storage, or during transport. In the case of a radionuclide, the inherited concentration will decrease with time due to decay. Inheritance concentrations will have less influence on exposure dating of very old landforms where $C \gg C_{inh}$, or in catchments with low TCN inventories due to very rapid erosion and transport rates, or for radionuclides with short mean lifetimes (e.g., ^{14}C). However, in landscapes where erosion is slow in terms of TCN production rate ($\bar{\varepsilon} \leq \bar{P}(0)\ \bar{\Lambda}/\rho t P(0)$, where the "bar" terms represent catchment-wide averages), in catchments with high relief where TCN production rates are in places much greater than that of the alluvium in question, or for young landforms, inheritance can have a significant control on the exposure age of the landform, and can exceed the in situ produced concentration.

[6] The shape of a depth-profile curve is characteristic of a given exposure age and time-integrated production rate, erosion history (or aggradation history), inheritance, mixing, and bulk density variation (and for thermal and epithermal neutron produced ^{36}Cl, volumetric water content and chemical composition). A depth profile of a single nuclide can provide the information needed to interpret the sediment age, surface erosion rate, and inheritance if the other parameters can be estimated or assumed negligible and if the sampled depth of the profile is sufficient to characterize both nucleogenic and muogenic production.

[7] A requirement for this depth-profile technique is that inheritance must be considered constant over the depth range of the samples [*Anderson et al.*, 1996]. That is, the deposit being analyzed must have been mixed well enough such that, at $t = 0$, a statistically large sample contains the same TCN concentration at every depth in the profile. However, variability in inheritance with depth is likely where deposition is incremental over significant time, where depositional processes vary in the profile, and where catchment-wide erosion rates vary significantly during the span of deposition.

2.2. Lees Ferry Sample Site

[8] To demonstrate the utility of this program, we use ^{10}Be data from an alluvial terrace at Lees Ferry, Arizona, which lies at the terminus of Glen Canyon and the head of Marble Canyon, leading to Grand Canyon (Figure 1). The relatively broad valley landscape here is developed where weak rocks are encountered at the confluence of the Colorado and Paria Rivers; this has allowed the preservation of a sequence of fill terraces. The sampled terrace lies atop the dominant Pleistocene alluvial fill at this location and is mapped as the M4 (main stem) Colorado River fill deposit [*Cragun*, 2007]. An advantage here is that the chronostratigraphy of this terrace sequence, and especially the M4 deposit, is established from several optically stimulated luminescence (OSL) dates [*Cragun*, 2007]. Specifically, bracketing OSL depositional ages indicate the sampled terrace was abandoned between 98 ± 10 and 77 ± 8 ka (2σ errors; J. L. Pederson, unpublished data, 2007). Thus, our model can be well tested with this example. It is not the purpose of this paper to discuss the relevance of this work for Grand Canyon geology as these matters have been dealt with elsewhere [e.g., *Pederson et al.*, 2002, 2006; *Polyak et al.*, 2008].

[9] To collect samples for this depth profile, a 2.5 m pit was hand-excavated in the center of the M4 terrace at 36.853°N, −111.606°W and 985 m above sea level. The pit was situated where the terrace surface is smooth and level, with no original bar-and-swale topography preserved. The sampled deposit is medium-bedded, clast supported, pebble-to-boulder gravel which in places is imbricated (Figure 2). Moderately strong desert soil development in the deposit is marked by rubification, clast weathering, and stage II calcic-horizon development in two Bk horizons. A Byk horizon with gypsum translocation extends to the bottom of the excavated soil pit. In addition, there is a moderately well

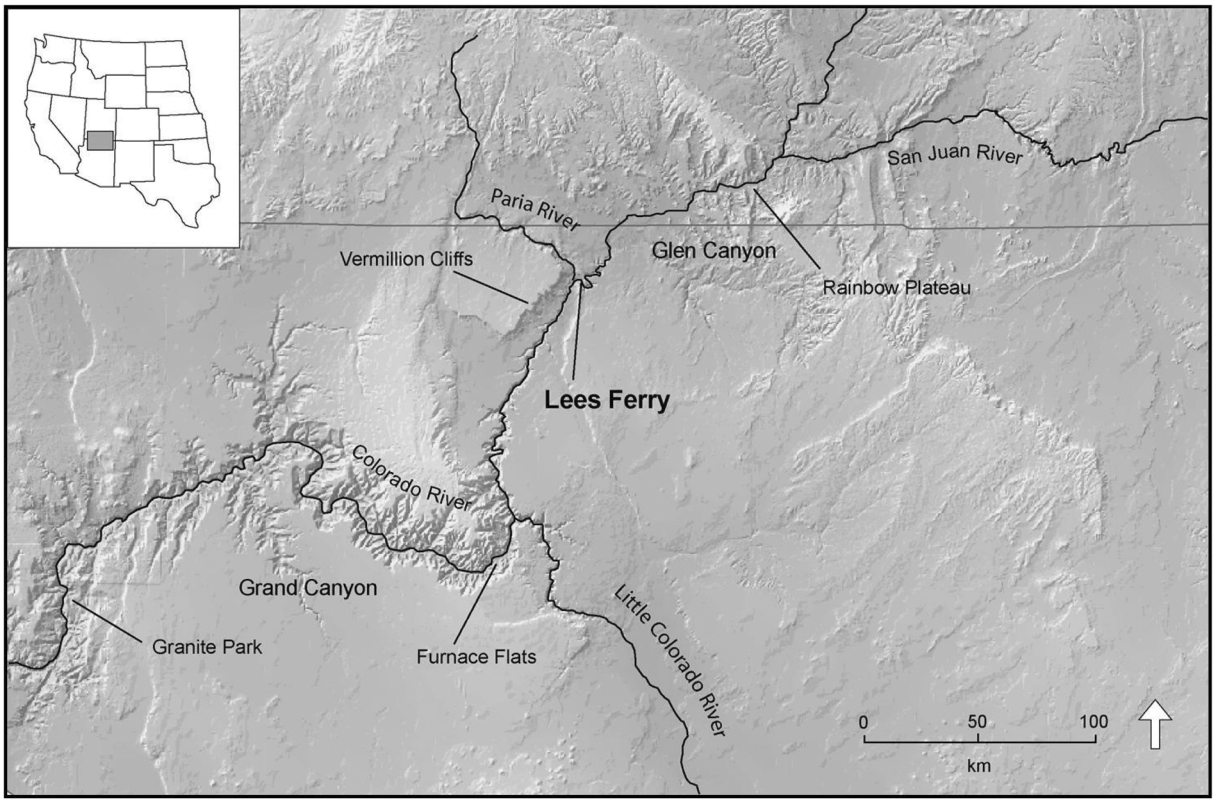

Figure 1. DEM of sample site at Lees Ferry, Arizona (modified from *Cragun* [2007]).

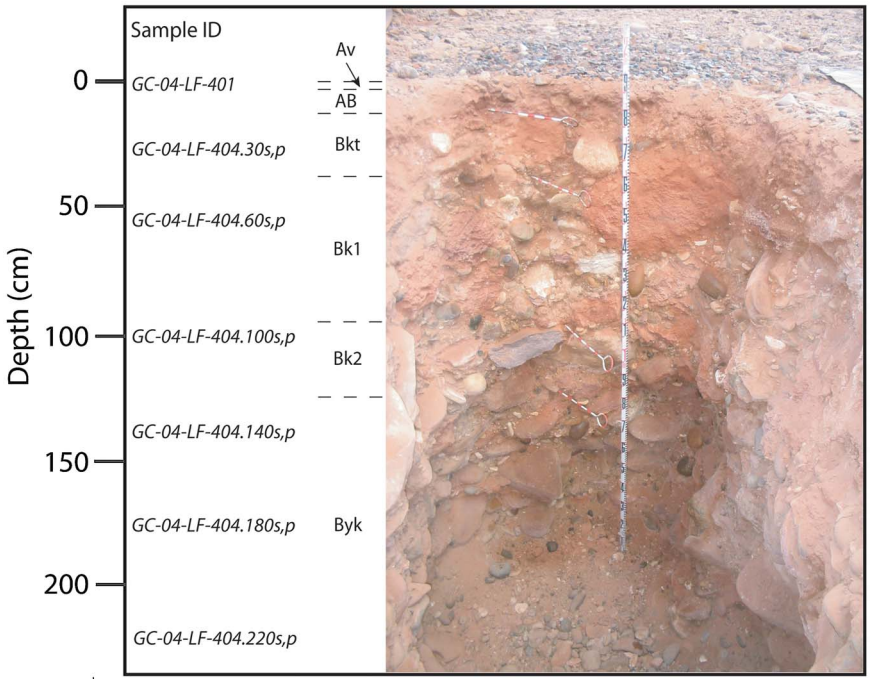

Figure 2. Photograph of excavated pit in M4 terrace at Lees Ferry, Arizona with identified soil horizons and TCN sample depths labeled (s, p = sand and pebble sample).

Table 1. Summary of Sample Data From the Lees Ferry M4y Terrace[a]

Sample ID	Depth (cm)	Thickness (cm)	Grain Size Range (μm)	Dissolved Mass (g)	Carrier Mass (g)	Corrected $^{10}Be/^{9}Be$	^{10}Be Concentration (atoms g^{-1})	1σ AMS Error (%)	1σ Total Measured Error (%)
GC-04-LF-401	0	1–3	10000–30000	40.3970	0.2982	1.7766E−12	858320	2.30	3.05
GC-04-LF-404.30s	27.5	5	295–500	45.2566	0.3080	1.2769E−12	568744	2.31	3.05
GC-04-LF-404.60s	57.5	5	355–500	45.9469	0.3000	9.5176E−13	406713	1.99	2.82
GC-04-LF-404.100s	97.5	5	295–710	50.1042	0.3123	7.1640E−13	292243	2.33	3.07
GC-04-LF-404.140s	137.5	5	295–710	51.1421	0.3034	5.2302E−13	203072	2.33	3.07
GC-04-LF-404.180s	177.5	5	295–710	55.3693	0.3085	4.3112E−13	157209	2.40	3.13
GC-04-LF-404.220s	217.5	5	355–710	55.1112	0.2974	3.7997E−13	134198	2.10	2.90
GC-04-LF-404.30p	27.5	5	10000–30000	20.4567	0.2820	8.3334E−13	751848	2.35	3.08
GC-04-LF-404.60p	57.5	5	10000–30000	27.0228	0.2784	7.1251E−13	480425	2.14	2.93
GC-04-LF-404.100p	97.5	5	10000–30000	22.2058	0.2703	3.2335E−13	257602	2.55	3.24
GC-04-LF-404.140p	137.5	5	10000–30000	30.5314	0.2764	3.4810E−13	206250	2.55	3.24
GC-04-LF-404.180p	177.5	5	10000–30000	27.3406	0.2725	4.7761E−13	311548	3.35	3.90
GC-04-LF-404.220p	217.5	5	10000–30000	23.0414	0.2705	1.0276E−12	789506	2.37	3.10

[a]Concentrations and errors were measured at the AMS facility at Lawrence Livermore National Laboratory; the total measurement error includes the AMS error added in quadrature with an estimated 2% 1σ error in sample preparation and analysis [see *Gosse and Phillips*, 2001]. All samples as well as a process blank were normalized with AMS standard KNSTD3110 and $^{10}Be/^{9}Be$ ratios were calculated using a ^{10}Be half-life of 1.387 Ma. ^{10}Be contribution from blank: 1.9×10^5 atoms (sand samples), 5.4×10^5 atoms (pebble samples).

developed desert pavement with interlocking angular pebbles of varnished chert, sandstone, felsic volcanics, and orthoquartzite overlying a 1–2 cm thick Av horizon. There is no evidence of buried or exhumed soil horizons. Based on these surface and subsurface soil features, and the lack of evidence for surface erosion within 15 m of the sample site, the surface is interpreted as very stable over at least Holocene time. However, the original depositional morphology is absent on the surface, some degree of bioturbation is evident, and development of an Av horizon under the pavement suggest the landform has experienced at least some modification, and probably net denudation, over late Quaternary time. We sampled approximately 2 kg of sediment for both pebbles and sand in the same pit to a depth of 220 cm below the M4 surface (Table 1). Details of sampling and processing are given in Appendix A and B.

3. Model Approach

[10] The depth profile simulator generates solutions to equation (1) using a constrained Monte Carlo approach designed to let the user input as much inferred or assumed information as necessary about the data set being analyzed. Probability distributions for pertinent parameters can be chosen depending on what is already known, assumed to be known, or believed about the sampled site. Additionally, constraints can be placed on coupled parameters to remove unrealistic scenarios from the parameter solution spaces. Afterward, remaining unknowns are simulated within the framework designated by the selected options (confidence limit, reduced chi-square cutoff). The following sections describe all the parameters the user can define, and how their entered distributions are handled. See readme.txt available at http://geochronology.earthsciences.dal.ca/downloads-models.html for general instructions and system requirements. The program is available for use in both Mathcad™ and Matlab™ environments and is easily modified to the user's choice of options and parameter distributions.

3.1. Parameters and Uncertainty

3.1.1. Surface Production Rate, P(0)

[11] A value of 4.76 atoms g^{-1} a^{-1} (*Stone* [2000] recalibrated according to *Nishiizumi et al.* [2007]) is set as the default ^{10}Be reference production rate at sea level and high latitude, which is scaled to the sample site using the *Lal* [1991] modified by *Stone* [2000] scaling scheme—a scheme based solely on measured latitude and atmospheric pressure (calculated from site altitude). Alternatively, the user can enter a spallogenic production rate determined using an independent method. There are several published scaling schemes, including more complicated ones that account for longitudinal or temporal variations in production due to geomagnetic field effects [e.g., *Dunai*, 2000; *Lifton et al.*, 2008].

Additionally, the user can specify the reference production rate used for the built in scaling scheme.

[12] The muogenic component of the surface production rate is calculated using the theoretical production equations of *Heisinger et al.* [2002a, 2002b]. We adopt the approach of *Balco et al.* [2008] to calculate muon production at a particular altitude and subsurface depth (in terms of mass-depth, g cm^{-2}). This approach assumes a negligible latitudinal effect on muon flux.

[13] The user is prompted to adjust the site production rate for topographic shielding, surface geometry, and any assumed periodic cover of, for example, snow, ash, or loess. If already known, these effects can be quantified by manually entering them as scaling factors (see *Gosse and Phillips* [2001] for details on calculating scaling factors). For topographic shielding and geometry, a combined scaling factor is calculated within the program by importing angular measurements of the horizon at specified azimuths as well as the strike and dip of the sampled surface. The angular distribution of cosmic flux is then integrated over the entire sky less the horizon to generate a combined scaling factor.

[14] The uncertainty of the surface production rate is relatively high. *Balco et al.* [2008] estimate that the 1σ error generated from empirical scaling schemes may be as high as 10%. Furthermore, by comparing production rate estimates using a variety of different scaling methods it is possible to quantify an additional uncertainty related to time-integrated geomagnetic field effects. Although this program allows the user to propagate a production rate error through to the solution spaces of all calculated parameters, it is often not useful to do so since i) it is straightforward and explicit to propagate this error through to parameter solution spaces classically, after the simulation is performed, ii) incorporating the large, systematic error in production rate can obscure the potentially useful Monte Carlo calculated probability distributions, iii) it is commonplace for authors not to incorporate the systematic production rate error in published results, so comparisons of error for published TCN measurements may not be useful, and iv) unnecessary imputed error distributions increase model run time—a potentially significant effect for larger simulations. Thus, the uncertainty in the production rate at the surface of the landform being analyzed can be ignored and added in quadrature to the Monte Carlo generated uncertainty after computation.

3.1.2. Cumulative Bulk Density, ρ_z

[15] Cumulative bulk density above each sample in a subsurface profile can be entered into the simulation in a variety of ways. For simple, homogeneous fills where cumulative bulk density may be presumed constant over the sampled depth range, high and low end-members can be imputed with a random distribution, or with a normal distribution defined in terms of a mean value and standard error if bulk density is known. For surfaces with a complicated relationship between cumulative bulk density and depth (e.g., older sediment with a well developed soil, or variations in sorting with depth), incremental measurements of bulk density within different horizons can be entered, each with their own user-defined normally distributed uncertainties. In circumstances where bulk density of a horizon may have changed significantly over time (e.g., eolian dust adding mass to an Av horizon [see *Reheis et al.*, 1995], or development of a petrocalcic horizon), an estimate for time-integrated bulk density and uncertainty should be employed. The imputed measurements and errors are used to create a depth-dependent normally distributed solution for cumulative bulk density, which is then integrated over the thickness of each sample in the profile to generate mean cumulative bulk density values with normally distributed errors at the depth range of each sample.

3.1.3. Erosion Rate, ε

[16] The shape of the upper few meters of a TCN depth profile is very sensitive to the age and erosion rate parameters and less so to inheritance. It is often necessary to provide constraint on erosion rate when modeling for an exposure age (or vice versa). Therefore, samples used for age and erosion rate estimates should be shallow whereas if precise estimates of inheritance are needed samples should span over a deeper profile. The degree and depth of mixing will control how shallow samples can be collected, although attempts to interpret TCN profiles in the mixed zone have also been made [*Perg et al.*, 2001]. The program is designed to allow simultaneous constraint of both net erosion and erosion rate. In the field it is often difficult to deduce reasonable erosion rates, although estimates for other parameters, such as net erosion, may be more easily interpreted from field observations—particularly for sediments with developed soils. For each depth profile solution generated, the erosion rate and age parameters are multiplied to yield a net erosion value, which must reside within the user-

defined net erosion constraint to be stored as a possible solution. The values for erosion rate can be sampled randomly between end-members, or normally about a mean value.

[17] Constraining aggradation at the top of a profile surface, or negative values for erosion rate and net erosion, is also permitted by this program so long as the profile samples are below the accumulation zone (otherwise the shallowest samples would not have been part of the profile since deposition). Changes in profile mass due to pedogenic processes (e.g., accretion of Bk or By horizons) are better treated separately, by assigning a time-averaged estimate of bulk density for those horizons (cf. previous section).

3.1.4. Other Parameters

[18] The options available for constraining age, inheritance, and the neutron attenuation length are similar. Each parameter can vary randomly between two end-members, or normally about a mean value. Unless the user has a priori knowledge of the age or inheritance, these parameters should vary randomly and over conservative end-members. A normally distributed mean value for the attenuation length of fast nucleons is suggested by the program based on the latitude of the sample site [*Gosse and Phillips*, 2001].

[19] All production coefficients for the five-term exponential approximation of the muogenic component are determined internally and represent a best fit to the theoretical muon production calculated by *Balco et al.* [2008] after *Heisinger et al.* [2002a, 2002b] at the site altitude and over a user-defined subsurface depth range. The default depth range is for 20 m of rock (~5400 g cm^{-2}), but can be extended to greater depths for deep profiles. The mean relative error of the fit is imposed as an error for the attenuation length coefficients; a normally distributed mean error in the total muogenic surface production rate can also be imposed by the user.

3.2. Data Inputs

[20] There are four measured data required by the program for each sample: TCN concentration, total measurement error in TCN concentration, sample depth, and sample thickness. This program does not reduce or standardize mass spectrometry or chemical data. Bulk density and topographic shielding may be measured or estimated as previously described. The total measurement error in TCN concentration should include the 1σ AMS uncertainty measurement as well as additional 1σ error associated with sample preparation and analysis (see *Gosse and Phillips*, 2001 for an estimate). Although uncertainty for these measurements is entered with 1σ confidence, the program allows the user to select higher confidence limits for the output. The uncertainties in measurement for the sample's depth and thickness need not be included since random errors affecting changes in sample spacing and thickness are very small when compared to the depth range of the measured profile, and any systematic error from an uncertainty in measuring the distance to the surface boundary of the profile (potentially significant for vegetated or irregular surfaces) can be included in a conservative estimate for the uncertainty in cumulative bulk density.

3.3. Profile Solutions

[21] After all parameter constraints are defined, parameter values are sampled from the assigned probability distributions to produce a solution to equation (1). The reduced chi-square statistic is then generated from each simulated profile solution. The reduced chi-square statistic is calculated as

$$\chi^2 = \frac{1}{d}\sum_{y=1}^{x}\frac{\left(\int_{T_y} C_m\left(z_y,\varepsilon,t\right)\,dz - N_{m,y}\right)^2}{\left(\sigma_{m,y}\cdot N_{m,y}\right)^2} \qquad (2)$$

where x is the number of samples in the profile, T_y is the thickness of indexed sample y (cm), $N_{m,y}$ is the measured concentration of nuclide m for sample y (atoms g^{-1}), $\sigma_{m,y}$ is the fractional standard error for $N_{m,y}$ (including all measurement errors), and d is the degrees of freedom in the data set—a value equal to the number of samples in the profile less the number of calculated parameters (to obtain statistically robust results, it is imperative that the number of samples analyzed in a depth profile be greater than the number of calculated parameters, thus a minimum of four samples is recommended to resolve solutions for age, erosion rate, and inheritance). A cutoff value is then determined from the chi-square probability distribution function

$$P(\chi_0) = \frac{2}{2^{d/2}\Gamma(d/2)}\int_{\chi_0}^{\infty} x^{d-1}\exp\left(-x^2/2\right)dx \qquad (3)$$

where $P(\chi_0)$ is the probability of finding a chi-square value greater than or equal to χ_0 [*Taylor*, 1997]. Profiles yielding a reduced chi-square statistic less than or equal to the cutoff value $P(\chi^2 \le \chi_0)$ are accepted, and their parameters are stored as possi-

ble solutions to the profile within a user-defined confidence window (e.g., 1σ, 2σ). The simulation continues until a specified number of generated profiles are found with reduced chi-square values lower than the cutoff. Although the cutoff is defined by the degrees of freedom permitted from the number of samples collected in the profile, the user is provided with the opportunity to define the chi-square value to, for instance, permit cursory interpretation of TCN depth data that cannot be fit due to excessive scatter or insufficient number of samples.

3.4. Model Constraints for Lees Ferry M4 Terrace

[22] A local spallogenic surface production rate of 9.51 atoms ^{10}Be (g SiO_2)$^{-1}$ a^{-1} was calculated for the Lees Ferry site using the *Stone* [2000] after *Lal* [1991] scaling scheme (reference production rate of 4.76 atoms g^{-1} a^{-1}), and accounting for topographic shielding (2.1% effect). The local total muogenic surface production rate was calculated to be 0.26 atoms ^{10}Be (g SiO_2)$^{-1}$ a^{-1}. The parameters for age, inheritance, and erosion rate were allowed to vary between conservative high and low values in order to avoid constraining by these parameters in the initial simulation. Net erosion of the M4 terrace surface was considered minimal and constrained between 0 and 30 cm. The fitted depth range for muon production was reduced to 5 m since this value is greater than the sum of our maximum allowed erosion and depth of deepest sample (a smaller depth range produces a better fit to the *Heisinger et al.* [2002a, 2002b] muon production equations). Since measurements of bulk density in the excavated soil pit returned values of 2.5 ± 0.2 g cm^{-3} at each measured depth (30, 60 and 205 cm) (a flimsy plastic bag was inserted into hole and filled with a measured quantity of water to determine the volume of excavated mass at each depth), cumulative bulk density was modeled as constant over the sampled interval. However, the authors believe these measured bulk density values should be considered a maximum since excavation of the very coarse boulder-gravel fill may have led to a systematic error in determining the volume of sediment excavated; a density approaching that of solid granite (2.7 g cm^{-3}) is unreasonable for a fluvial deposit. Thus, cumulative bulk density was treated as constant with depth, but allowed to vary randomly between 2.2 and 2.5 g cm^{-3}. A normally distributed mean value of 160 g cm^{-2} with a 3% standard error was used for the neutron attenuation length. See Table 2 for a summary of the Lees Ferry model constraints and Figure 3 for a snapshot of the data entered into the Matlab™ graphical user interface. Each simulation continued until 100,000 profile solutions were obtained.

4. Results

4.1. Lees Ferry Sand Profile

[23] The ^{10}Be data for the six sand samples (see Table 1) were modeled using the constraints shown in Table 2. These data permitted solutions that exceeded the chi-square cutoff for the 95% (2σ) confidence window and exhibited a well-behaved exponential decrease in ^{10}Be concentration with depth (Figure 4a); only solutions at or below this value were retained for analysis in order to appropriately propagate error through to the calculated parameters. Because of our imposed constraint on net erosion, the erosion rate solution space is truncated, and thus is not useful for estimating an erosion rate (Figure 5). The six sample simulation yields modal values of $83.9^{+19.1}_{-14.1}$ ka, and $9.49^{+1.21}_{-2.52} \times 10^4$ atoms g^{-1} for age and inheritance, respectively (Table 3 and Figure 5).

[24] Although a minimum chi-square value is returned for the set of curves generated by the simulation, comparison of the solution space for age and associated chi-square values (Figure 5) demonstrates that, for this profile, optimization will not converge to a single solution. These results show a wide range of ages with chi-square values essentially identical to the minimum chi-square value. That is, as the chi-square value decreases to the minimum value allowed by this data set, the resulting age does not approach a unique value. This is in contrast to the inheritance solution space (Figure 5) which does converge to a unique solution as chi-square value decreases. Examination of the resulting age and erosion rate pairs in an unconstrained simulation further demonstrates no relationship between minimized chi-square and age; Figure 6 shows that any age greater than ~70 ka is equally likely to be obtained from an optimization algorithm. Therefore, for this data set, without some constraint on either net erosion or erosion rate only a minimum age can be resolved.

4.2. Lees Ferry Pebble Profile

[25] The measured TCN concentrations for the sand profile produce a theoretical exponential distribution with depth in concordance with equation (1); the pebble profile, however, does not demonstrate

Table 2. Summary of User Options Available for Simulation[a]

Parameter	Value	Unit	Description
Location data			
Latitude	36.852	deg	latitude of profile site in decimal degrees
Longitude	−111.606	deg	longitude of profile site in decimal degrees
Altitude	985	m	site altitude
Strike	0	deg	strike of surface (0–360 deg)
Dip	0	deg	dip of surface (0–90 deg; right hand rule)
Shielding data			
Azimuths	0[b]	deg	data are imported from ASCII text file; first column with azimuth measurements, second column with corresponding angle to horizon
Angles	15[b]	deg	see description of azimuths
Sample data			
Depths	27.5[b]	cm	data are imported from ASCII text file with four columns of data in the following order: depths (depth to top of each sample), thicknesses (sample thickness), sample concentrations, error in measurement. See Table 1 for suite of data used for simulation
Thickness	5[b]	cm	see description of depths
Isotope concentration	568744[b]	atoms g^{-1}	see description of depths
Measurement error	0.0305[b]	fraction	see description of depths
Density data			
Depth dependent			
Depths	NA[b]	cm	data are imported from ASCII text file with three columns of data in the following order: depths (to top of each horizon–always starts with 0), horizon densities, and estimated uncertainty in density measurement
Densities	NA[b]	g cm^{-3}	see description of depths
Individual uncertainties	NA[b]	g cm^{-3}	see description of depths
Depth constant			
Option 1: constant value	NA	g cm^{-3}	density is constant with depth, and it's value is fixed
Option 2: mean value	NA	g cm^{-3}	density is constant with depth, but value varies with a normal distribution about a mean value
std	NA	g cm^{-3}	see description of mean value
Option 3: max value	2.5	g cm^{-3}	density is constant with depth, but varies randomly between two end-member values
min value	2.2	g cm^{-3}	see description of max value
Spallogenic production			
Option 1: manual entry	NA	atoms g^{-1} a^{-1}	enter a production rate calculated from some other source
Option 2: internally calculated	9.51	atoms g^{-1} a^{-1}	production rate calculated from *Stone* [2000] after *Lal* [1991]
Reference production rate	4.76	atoms g^{-1} a^{-1}	from *Stone* [2000] recalibrated after *Nishiizumi et al.* [2007]; user can edit
Uncertainty			
Option 1: constant value	9.51	atoms g^{-1} a^{-1}	surface production rate is constant
Option 2: mean value	NA	atoms g^{-1} a^{-1}	surface production rate varies with a normal distribution about a mean value
std	NA	atoms g^{-1} a^{-1}	see description of mean value
Option 3: max value	NA	atoms g^{-1} a^{-1}	surface production rate varies randomly between two end-member values
min value	NA	atoms g^{-1} a^{-1}	see description of max value
Neutron attenuation			
Option 1: constant value	NA	g cm^{-2}	neutron attenuation length is constant
Option 2: mean value	160	g cm^{-2}	neutron attenuation length varies with a normal distribution about a mean value
std	5	g cm^{-2}	see description of mean value

Table 2. (continued)

Parameter	Value	Unit	Description
Option 3: max value	NA	g cm^{-2}	neutron attenuation length varies randomly between two end-member values
min value	NA	g cm^{-2}	see description of max value
Muon production			
Depth of production fit	5	m	depth of curve fit to muon production of *Balco et al.* [2008] after *Heisinger et al.* [2002a, 2002b]; total uncertainty for fast and negative muons
Total uncertainty	0	(%)	see description of depth of production fit
Isotope half-life			
Uncertainty in half-life	5	(%)	estimated uncertainty in half-life
Age			
Option 1: constant value	NA	a	age is treated as constant during simulation (useful for sensitivity analyses)
Option 2: mean value	NA	a	age varies with a normal distribution about a mean value (independent age measurement)
std	NA	a	see description of mean value
Option 3: max value	40,000[c]	a	age varies randomly between two end-member values (end-members should be conservative enough to not constrain simulation)
min value	150,000[c]	a	see description of max value
Erosion			
Net erosion			
Max value	30	cm	maximum erosion estimated from site (use large value if unknown)
Min value	0	cm	minimum erosion estimated from site (can be negative for aggradation)
Erosion rate			
Option 1: constant value	NA	cm ka^{-1}	erosion rate is treated as constant during simulation (useful for sensitivity analyses)
Option 2: mean value	NA	cm ka^{-1}	erosion rate varies with a normal distribution about a mean value (independent erosion rate measurement)
std	NA	cm ka^{-1}	see description of mean value
Option 3: max value	0.4[c]	cm ka^{-1}	erosion rate varies randomly between two end-member values (end-members should be conservative enough to not constrain simulation; must not contradict net erosion cut-offs)
min value	0	cm ka^{-1}	see description of max value
Inheritance			
Option 1: constant value	NA	atoms g^{-1}	inheritance is treated as constant during simulation (useful for sensitivity analyses)
Option 2: mean value	NA	atoms g^{-1}	inheritance varies with a normal distribution about a mean value (independent inheritance measurement)
std	NA	atoms g^{-1}	see description of max value
Option 3: max value	50,000[c]	atoms g^{-1}	inheritance varies randomly between two end-member values (nonnegative values only; conservative end-members can usually be estimated from deepest sample)
min value	150,000[c]	atoms g^{-1}	see description of max value
MC settings			
Option 1: chi-square cut-off	NA	NA	only accepts profile solutions with a lower reduced chi-square value
Option 2: sigma confidence	2	NA	only accepts profile solutions within specified sigma confidence
Parallel processing?	Y	NA	allows parallel utilization of multiple core and processor machines (see readme.txt)
Profile solutions	100,000	NA	number of acceptable solutions to generate before simulation ends

[a]Data and simulation parameters shown are those entered for the Lees Ferry sand profile.
[b]Not entered as a single value, but as a column matrix of data from an ASCII text file; value shown is one example.
[c]Value is a boundary condition and a conservative estimate for the particular end-member; efficient end-members are determined iteratively (see Appendix C).

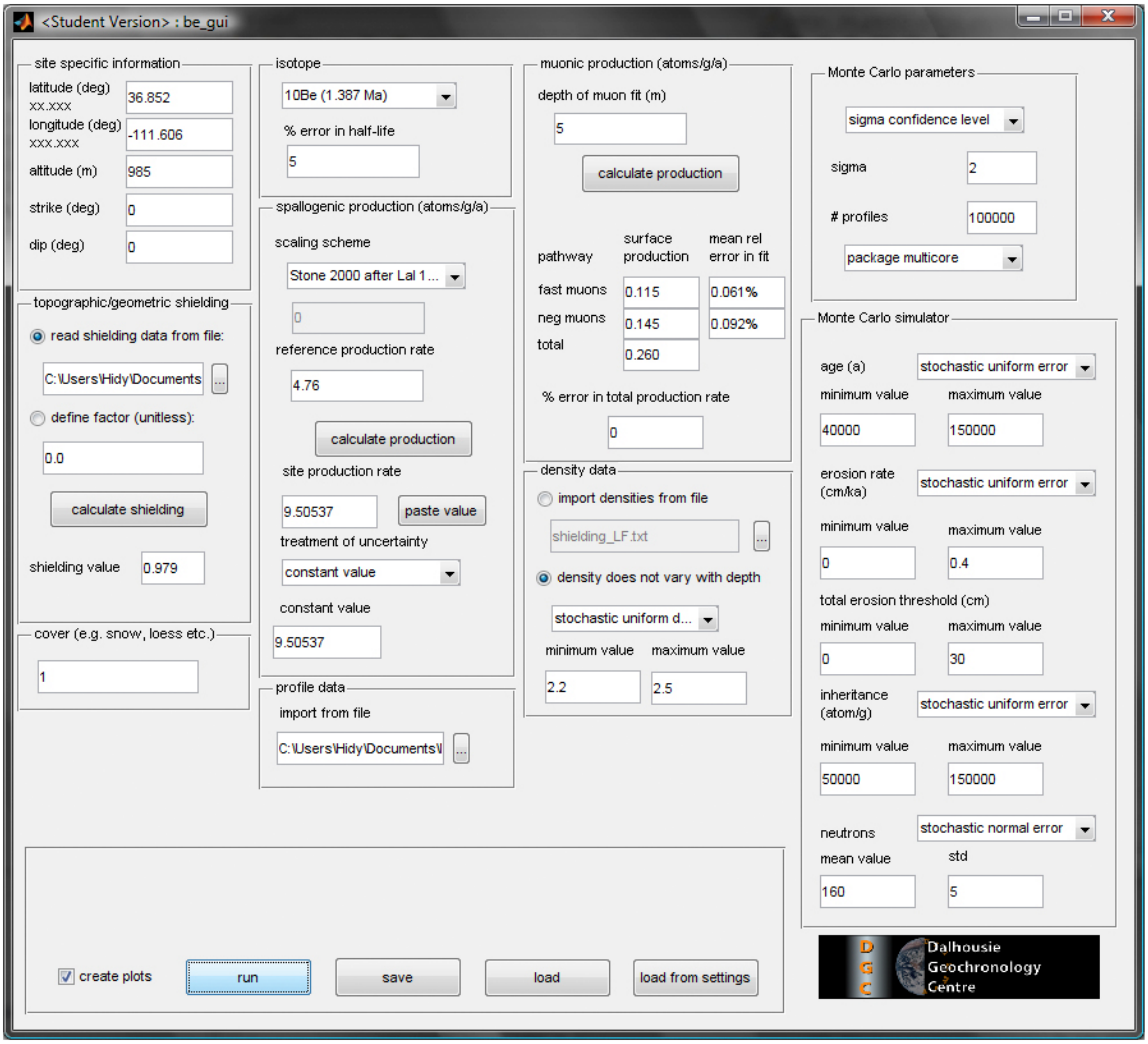

Figure 3. Snapshot of the graphical user interface for the Matlab™ version of this program.

an exponential decrease in TCN concentration with depth (Figure 4b). In particular, the ^{10}Be concentrations of the deepest two samples in the pebble profile deviate significantly from the theoretical profile shape that the upper four follow. Because of such an extreme deviation (~75% and ~500% from the expected concentrations based on the trend of the upper four), these two deepest pebble samples could not be included in the model, as it is apparent that no solution would satisfy all six samples.

[26] The ^{10}Be data for the four uppermost pebble samples (see Table 1) were modeled using the same model constraints as those imposed on the sand samples since they were collected in the same pit. For these samples, no solution existed at or below the chi-square cutoff for the 95% (2σ) confidence window. Thus, to obtain some result, the chi-square cutoff was manually increased to look at the distributions for each parameter's solution space based on the collection of best possible fits to the data. Although this cripples our ability to quantify error in the calculated parameters using equation (3), it still allows the determination of most probable (modal) values based on the data. The simulation yields modal values of 117 ka, and 4.60×10^4 atoms g^{-1} for age and inheritance, respectively (Table 4 and Figure 7).

5. Discussion

5.1. Interpreting Results With This Program

[27] Depending on the quality of the data set being analyzed, this profile simulator can be used in

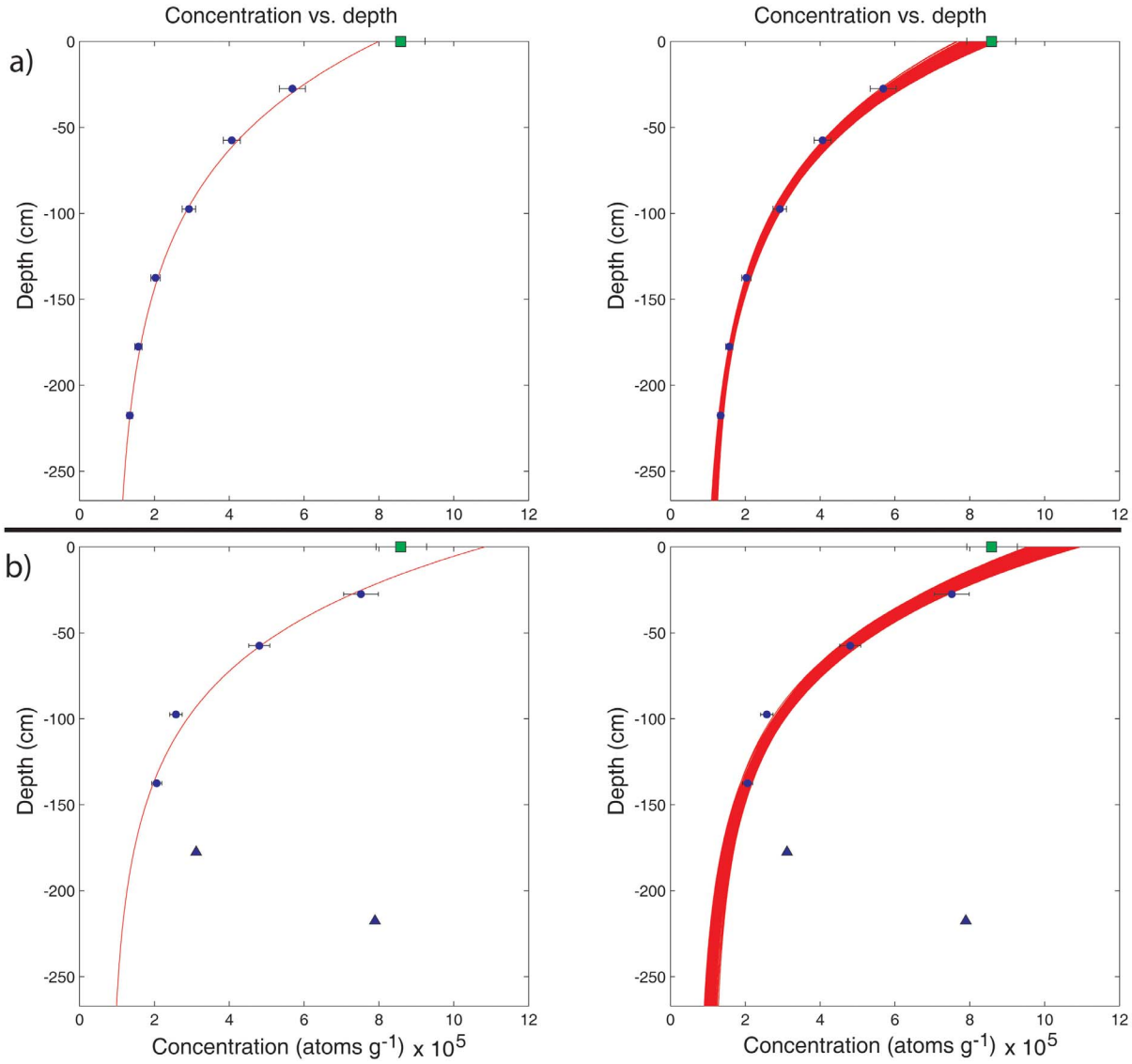

Figure 4. Concentration versus depth plots illustrating the (right) 2σ profile solution spaces and (left) best fits to equation (1) for (a) the sand profile and (b) the pebble profile. Error bars represent 2σ total measurement error (see Table 1). The lower two samples in the pebble profile (blue triangles) were not part of the simulation due to extreme discordance with the theoretical change in nuclide concentration with depth. The green square represents an amalgamated desert pavement sample; this sample was not included in any simulation since erosion may have changed its position with respect to the other samples in the profile.

different ways. For data where equation (1) provides sufficient solutions within the desired confidence window, it is straightforward to enter appropriate parameter constraints, run the simulation, obtain desired statistics on the parameter solution spaces, and report an age. Maximum and minimum values would represent the upper and lower 2σ error in age. However, in some sediment TCN concentrations may vary sporadically with depth or perhaps the profile contains fewer samples than the four needed to use equation (3) to calculate a chi-square cutoff. In those circumstances a rigorous treatment of error is not possible with this program; however, the model can still be used to generate modal values for the calculated constraints. For the case of data that are broadly scattered with depth, the chi-square cutoff can be manually increased until a desired number of profile solutions can be generated (as was done for the Lees Ferry pebble profile). This allows the user to view and collect the best possible fits to the data and ascertain if the calculated parameters converge

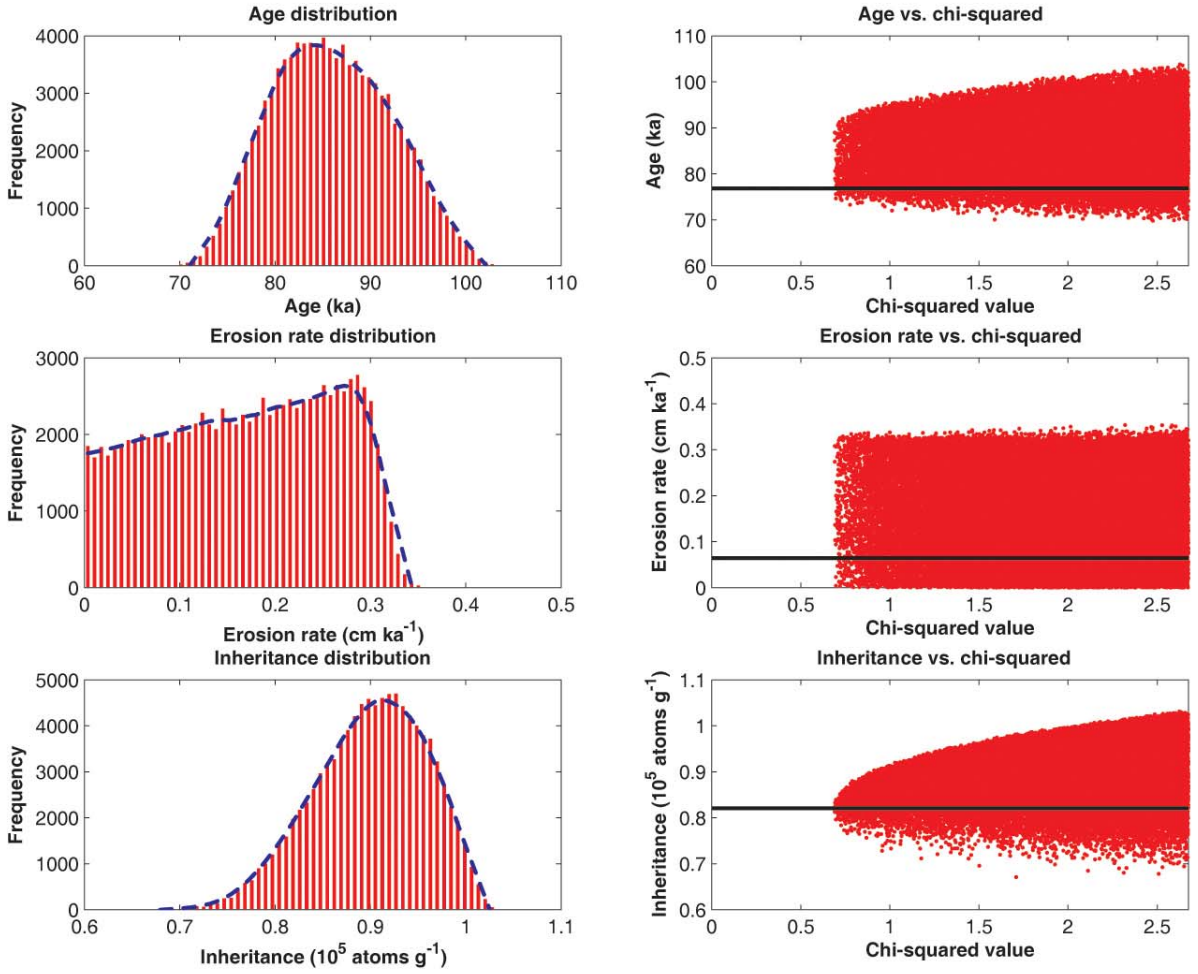

Figure 5. Results for the 2σ age, inheritance, and erosion rate solution spaces for the six sample sand profile in the Lees Ferry M4y terrace. Solid black lines indicate the lowest chi-square value. The chi-square cutoff was obtained from equation (4). Statistics for this simulation are shown in Table 3.

to a solution. We stress, however, that any solutions obtained via this approach cannot be quoted with an uncertainty as such data violate the model's assumption that inheritance is constant with depth. For sparse data ($d < 1$) that is not broadly scattered with depth, we recommend setting the chi-square cutoff to the number of samples in the profile. This results in parameter solution spaces defined by curves with a lower chi-square value than that of pseudo-data existing at the maximum error for each measured sample; this approach should yield a conservative estimate of error in the calculated parameters.

5.2. Age of the Lees Ferry M4 Terrace

[28] The most probable exposure age for the abandonment of the M4 terrace is $83.9^{+19.1}_{-14.1}$ ka based on the six-sample sand profile. The maximum and minimum simulated values of 103 ka and 69.8 ka represent our 2σ confidence limits for this age (+23% and −17%, respectively). This incorporates all relevant sources of error except the poorly known systematic errors in spallogenic and muogenic production rates. This result agrees with independent OSL-derived depositional ages that bracket the exposure age between 98 ± 10 and 77 ± 8 ka (2σ errors). We reject the results of the pebble profile data, which yield a modal age of 117 ka, for several reasons: i) the lowest two samples in the profile do not agree with the theoretical relationship between ^{10}Be concentration and depth (which was demonstrated by the sand profile, indicating that there is no mixing of sediment) (Figure 4b), ii) the remaining four samples that appeared to agree with this theoretical relationship did not pass the chi-square test at the 95% confidence window—

Table 3. Statistics for the Simulation of the Six Sample Sand Profile[a]

	Age (ka)	Inheritance (10^4 atoms g^{-1})	Erosion Rate (cm ka^{-1})
Mean	86.0	9.35	0.17
Median	85.7	9.40	0.18
Mode	83.9	9.49	0.28
Lowest χ^2	76.8	8.21	0.06
Maximum	103.8	10.7	0.35
Minimum	69.8	6.97	0.00

[a]Maximum and minimum values represent the 95% (2σ) confidence window for each parameter for the sand data; for the pebble data a cutoff of $\chi^2 \leq 30$ was imposed and therefore no reasonable uncertainty can be obtained from the simulation. Statistics are shown for erosion rate; however, since constraint was placed on net erosion they cannot be used to report a value for erosion rate.

implying less than a 5% probability that these data are governed by the expected distribution of equation (1), iii) the number of individual clasts acquired for the amalgamated pebble samples (150–200) was much less than that acquired for the sand samples (~10^7); thus, the pebble samples produce statistically weaker results along with an increased potential for ^{10}Be within a single clast to dominate the amalgamated concentration, and iv) the pebble age result is significantly older than the independent geochronologic constraints at the site.

[29] Interestingly, the ^{10}Be concentration of the desert pavement sample at the surface is in complete agreement with the modeled surface concentrations from the sand profile (Figure 4a); this supports the field interpretation that the terrace surface has been relatively stable over the duration of exposure, with negligible denudation over time, and may have implications for the longevity of desert pavement stability.

5.3. Implications for Sampling TCN Depth Profiles

[30] The Monte Carlo-constrained program can help devise sampling strategies for TCN depth profiles and assist the interpretation of their data. For example, the model can be run in a forward style to test the sensitivity of parameters, calculate optimal sample depths, and test the feasibility of exposure dating a particular site.

[31] The deviation between the Lees Ferry sand and pebble data is an important result that should guide

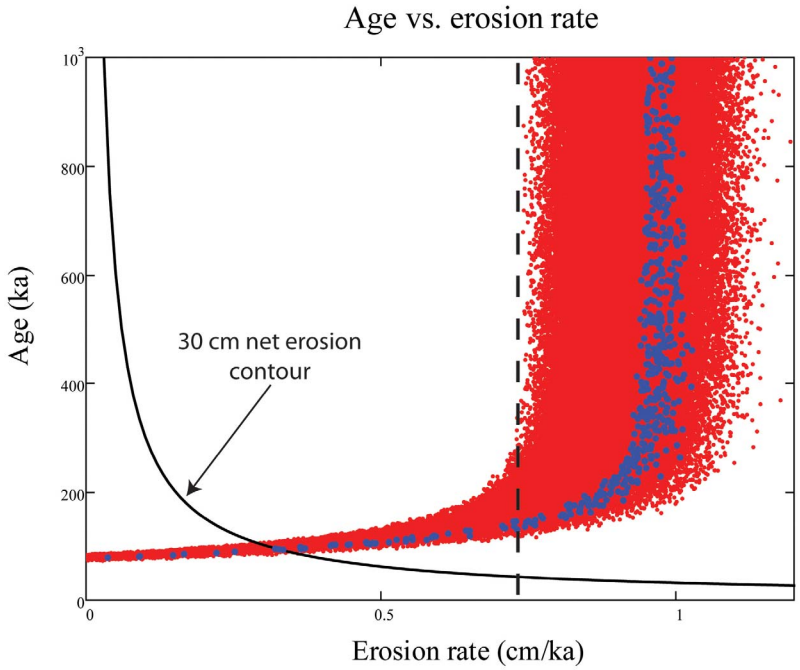

Figure 6. Age-erosion rate plot for a sand profile simulation with no erosion constraint. Small red dots define the solution space; large blue dots mark the 500 best (lowest chi-square) solution pairs (out of 100,000). The solid black curve marks the 30 cm net erosion cutoff for our sample site. The dashed black line marks the erosion rate cutoff that would be needed to resolve a finite age. Notice 1) that the lowest chi-square solutions are broadly scattered with respect to age, and 2) that without a constraint on erosion (or erosion rate), only a lower age limit can be determined for this data set.

Table 4. Statistics for the Simulation of the Four Sample Pebble Profile[a]

	Age (ka)	Inheritance (10^4 atoms g^{-1})	Erosion Rate (cm ka^{-1})
Mean	121	5.24	0.12
Median	121	5.09	0.12
Mode	117	4.78	0.20
Lowest χ^2	139	7.67	0.17
Maximum	157	10.6	0.24
Minimum	98.6	2.43	0.00

[a]Maximum and minimum values represent the 95% (2σ) confidence window for each parameter for the sand data; for the pebble data a cutoff of $\chi^2 \leq 30$ was imposed and therefore no reasonable uncertainty can be obtained from the simulation. Statistics are shown for erosion rate; however, since constraint was placed on net erosion they cannot be used to report a value for erosion rate.

future profile sampling. Since the pebble and sand samples acquired from the excavated soil pit were collected from the same horizons, the post-depositional production of ^{10}Be in both the sand and pebble samples should be the same. The results, however, are widely different—especially for the two lowest samples. Since the sand data yield a tight concentration versus depth relationship, we exclude the possibility of post-depositional mixing. Instead, either our lower pebble samples are not representative of the average inherited TCN concentration, or the assumption that the TCN inventory is constant with depth is invalid. We cannot preclude unrecognized error in chemistry or AMS measurement, but we believe this is unlikely considering the precision of the measurements and process blank. Although *Repka et al.* [1997] suggested that an amalgamated pebble sample of 30 or more clasts is sufficient to provide a representative average TCN concentration, this may not be true for all alluvial deposits, particularly those in arid environments. First, a much higher variability of clast-specific inheritance concentrations is to be expected in sediment sourced by catchments with overall low

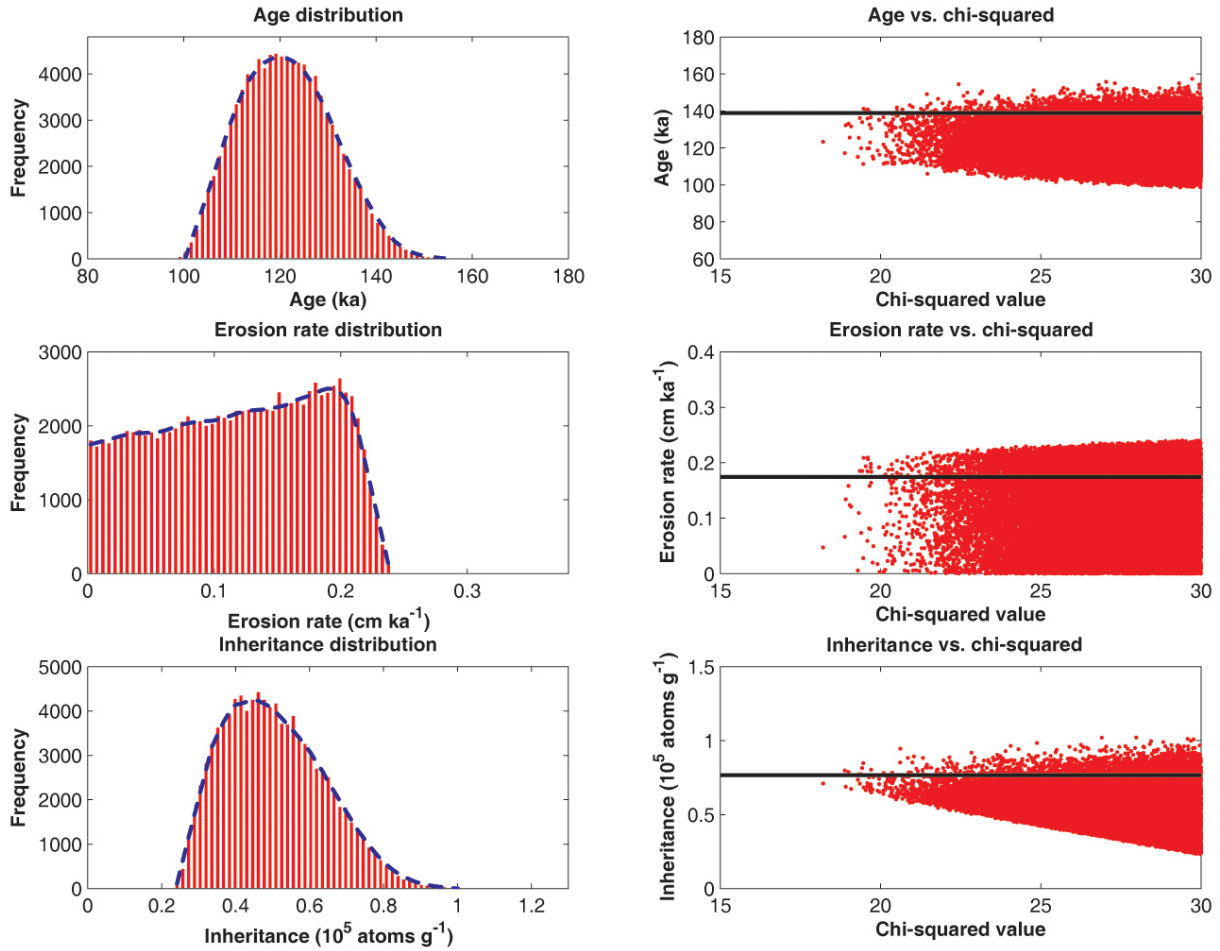

Figure 7. Results for age, inheritance, and erosion rate solution spaces for the four sample pebble profile in the Lees Ferry M4y terrace. Solid black lines indicate the lowest chi-square value. A chi-square cutoff of 30 was artificially imposed to generate these distributions. The statistics for this simulation are shown in Table 4.

rates of denudation. Second, mixing of gravel clasts is likely to be less complete than mixing of sand. We recommend always sampling sand if available and emphasize caution when sampling pebbles for TCN depth profiles because the probability of a constant inherited TCN concentration with depth likely decreases with increasing grain size.

[32] For ^{36}Cl depth profiles, procedures outlined by *Kirby et al.* [2006] provide a thorough means of considering the effect of soil moisture. However, the added complication of a depth variation in thermal neutron flux due to chemical variations in the soil profile must also be considered when sampling. If the thermal neutron component is unavoidable, or if it is sought due to the extra sensitivity of the cumulative thermal neutron profile to surface erosion, then collecting swaths of sediment above each sample should be considered in order to provide a more thorough means of establishing elemental abundances of thermal neutron absorbers and producers throughout the profile. A version of the MathCad™ profile code for interpreting ^{36}Cl depth profiles is available online; a Matlab™ version is currently being coded.

6. Conclusions

[33] This program allows the performance of rapid, simple, and comprehensive Monte Carlo simulations of TCN depth profiles which can be constrained from knowledge of the geology at the collection site. Additionally, it permits an explicit propagation of all error sources to calculated values for age, inheritance, and erosion rate.

[34] Results generated from simulating a sand profile from the Lees Ferry M4 terrace are robust, and agree with independent OSL chronology. However, a simulation performed on the Lees Ferry sand profile without constraint on erosion yields a non-unique and non-finite age (Figure 6). This indicates that without constraint on erosion rate or age, neither parameter can be resolved with a shallow depth profile (specific to TCNs without production from thermal and epithermal neutrons).

[35] Concentrations from a pebble profile (derived from the same pit as a sand profile) indicate that grain size can significantly influence age models due to the higher probability of poor mixing and higher contributions of inheritance from individual larger clasts during deposition.

[36] Because many different profile curves (reflecting uncertainty in variation of density and inheritance with depth) can explain TCN concentrations measured in the subsurface, the total uncertainty in ages estimated from depth profile studies is higher than normally reported using a minimum chi-square optimization approach or a simpler curve fitting method. This intrinsic error analysis better reflects the true uncertainty of TCN dating with depth profiles.

Appendix A: Lees Ferry—Specific Sampling Methods

[37] A 250 cm pit was hand-excavated in the M4 terrace and six ~1 kg samples of both sand and pebbles were collected at regular depth intervals of 30–40 cm (Figure 2). Depth contours were marked by a level line nailed into the pit walls, and the samples were collected from a ±2.5 cm swath along each contour. Sand samples were sieved in the field to remove the coarse (>2 mm) grains, then later sieved to the desired size range (Table 1); pebble samples (~1–3 cm) with high quartz content were collected indiscriminately, but consisted primarily of chert and quartzite. Each pebble sample consisted of ~150–200 individual clasts. Additionally, one amalgamated surface sample of the desert pavement was collected in a fashion identical to that of the other pebble samples. The physical and chemical sample preparation procedures used for all samples at Dalhousie Geochronology Centre are provided in Appendix B. From 20–60 g of pure quartz per sample, the thirteen ^{10}Be targets (plus two process blanks) were mixed 1:1 with niobium powder, packed in stainless steel target holders, and analyzed at the Center for Accelerator Mass Spectrometry at Lawrence Livermore National Laboratory.

Appendix B: Laboratory Methods

[38] Sand samples were sieved to extract the 355–500 μm range; the desert pavement and other pebble samples were crushed, and then sieved to extract this same size range in order to accelerate digestion. Ranges were expanded to 295–710 μm for samples that did not contain enough mass in the 355–500 μm bin. All samples were processed at the Dalhousie Geochronology Centre, AMS measurements were completed at CAMS-LLNL, and the resulting ^{10}Be concentrations are reported in Table 1.

[39] Each sample was subjected to the following laboratory procedures outlined in the DGC-CNEF laboratory manual (http://cnef.earthsciences.dal.ca):

aqua regia (3:1 of HCl:HNO_3), HF etching, ultrasonic quartz separation, magnetic separation, sand abrasion, and hand picking. These procedures purified the samples to ~99% quartz, dissolved aggregate grains and weak silicates, and removed any atmospheric ^{10}Be adsorbed to the grain surfaces. Approximately 0.2 mg of Be carrier was added to each sample to facilitate AMS by isotope dilution. The carrier was produced by J. Klein from a shielded beryl crystal extracted from the Homestake Gold Mine and has a long-term average $^{10}Be/^{9}Be$ of 4×10^{-15} at LLNL. Additionally, two process blanks were analyzed and used to subtract any background concentration, which in all instances was <10% the adjusted value. The samples were digested in a HF-$HClO_4$ mixture and the Be^{+2} cation extracted via ion chromatography. After precipitating the Be^{+2} cation at pH 9.2 with ultrapure ammonia gas, the samples were baked in a furnace at 850°C for one hour to produce a small amount of beryllium oxide powder—which was mixed 1:1 with niobium and sent to Lawrence Livermore National Laboratory for AMS analysis.

Appendix C: Model Run Time

[40] It is difficult to categorically state the time it will take for this simulator to adequately model a given data set as the duration will depend on the quality of the data set, how tightly the various pertinent parameters can be constrained, the desired confidence window of the calculated results, and also, of course, the computer used to run the program. However, once the user has set all parameters and constraints, an estimate can be made by performing a quick test run with a low number of desired profiles (we suggest ~1000). This allows the user to extrapolate the duration for a much larger simulation, as processing speed is linear, and, more importantly, get a better sense of how well the constraints imposed on the calculated parameters agree with the data. For example, say the exposure age of a given surface is unknown and that the user can only say confidently that it is somewhere between 5–500 ka. After a quick test run with this age range, however, it is seen that no solutions exist outside of an age range of 50–100 ka. The user should then feel comfortable further constraining the age window, keeping in mind that a distribution generated from a low number of simulated profiles will only yield a rough estimate for the age window boundaries. Constraining the simulated age window to, say, 20–150 ka would probably then be justified and would also speed up the run time for the larger simulation. On the contrary, if any test simulation (or full simulation) yields solutions at either boundary of a calculated parameter window, then that parameter window should be expanded accordingly unless the user has some reason to constrain it.

Acknowledgments

[41] Thanks to G. Yang for support in the Dalhousie Geochronology Centre cosmogenic nuclide lab. We appreciate the support of the staff of the LLNL-CAMS during the AMS runs, J.-L. Antinao for early discussions on the model, and E. McDonald for insights from soils geomorphology. J. Stone and G. Balco, and F. Phillips provided Matlab- and Excel-based codes for ^{10}Be and ^{36}Cl, respectively. Thanks to F. Phillips, S. Marrero, and B. Borchers for evaluating the Beta version of the ^{36}Cl depth profile code and providing extremely helpful feedback. We benefited from comments by two anonymous and thorough reviews on a previous version of the manuscript (and code). The Matlab™ Central database provided several code packages used by our simulator (datatablepackage, herrorbar, and multicore). The authors acknowledge funding from the following sources: JCG: AIF-100-1052, CFI, NSERC Discovery Grant, NSF-EAR9903126. JP: NSF-EAR 0346054.

References

Anderson, R. S., J. L. Repka, and G. S. Dick (1996), Explicit treatment of inheritance in dating depositional surfaces using in situ ^{10}Be and ^{26}Al, *Geology*, *24*, 47–51, doi:10.1130/0091-7613(1996)024<0047:ETOIID>2.3.CO;2.

Balco, G., J. O. Stone, N. A. Lifton, and T. J. Dunai (2008), A complete and easily accessible means of calculating surface exposure ages or erosion rates from ^{10}Be and ^{26}Al measurements, *Quat. Geochronol.*, *3*, 174–195, doi:10.1016/j.quageo.2007.12.001.

Braucher, R., P. Del Castillo, L. Siame, A. J. Hidy, and D. L. Bourles (2009), Determination of both exposure time and denudation rate from an in situ-produced 10Be depth profile: A mathematical proof of uniqueness. Model sensitivity and applications to natural cases, *Quat. Geochronol.*, *4*, 56–67, doi:10.1016/j.quageo.2008.06.001.

Brocard, G. Y., P. A. van der Beek, D. L. Bourles, L. L. Siame, and J.-L. Mugnier (2003), Long-term flivial incision rates and postglacial river relaxation time in the French Western Alps from ^{10}Be dating of alluvial terraces with assessment of inheritance, soil development and wind ablation effects, *Earth Planet. Sci. Lett.*, *209*, 197–214, doi:10.1016/S0012-821X(03)00031-1.

Cragun, W. S. (2007), Quaternary evolution of the Colorado River at Lees Ferry, Arizona, Master's thesis, 195 pp., Utah State Univ., Logan.

Dunai, T. J. (2000), Scaling factors for production rates of in situ produced cosmogenic nuclides: A critical reevaluation, *Earth Planet. Sci. Lett.*, *176*, 157–169, doi:10.1016/S0012-821X(99)00310-6.

Gosse, J. C., and F. M. Phillips (2001), Terrestrial in situ cosmogenic nuclides: Theory and application, *Quat. Sci. Rev.*, *20*, 1475–1560, doi:10.1016/S0277-3791(00)00171-2.

Granger, D. E., and A. L. Smith (2000), Dating buried sediments using radioactive decay and muogenic production of ^{26}Al and ^{10}Be, *Nucl. Instrum. Methods Phys. Res., Sect. B*, *172*, 822–826, doi:10.1016/S0168-583X(00)00087-2.

Heisinger, B., D. Lal, A. J. T. Jull, P. Kubik, S. Ivy-Ochs, S. Neumaier, K. Knie, V. Lazarev, and E. Nolte (2002a), Production of selected cosmogenic radionuclides by muons: 1. Fast muons, *Earth Planet. Sci. Lett.*, *200*, 345–355, doi:10.1016/S0012-821X(02)00640-4.

Heisinger, B., D. Lal, A. J. T. Jull, P. Kubik, S. Ivy-Ochs, K. Knie, and E. Nolte (2002b), Production of selected cosmogenic radionuclides by muons: 2. Capture of negative muons, *Earth Planet. Sci. Lett.*, *200*, 357–369.

Kirby, E., D. W. Burbank, M. Reheis, and F. Phillips (2006), Temporal variations in slip rate of the White Mountain Fault Zone, eastern California, *Earth Planet. Sci. Lett.*, *248*, 168–185, doi:10.1016/j.epsl.2006.05.026.

Lal, D. (1991), Cosmic ray labeling of erosion surfaces: In situ nuclide production rates and erosion models, *Earth Planet. Sci. Lett.*, *104*, 424–439, doi:10.1016/0012-821X(91)90220-C.

Lifton, N., D. F. Smart, and M. A. Shea (2008), Scaling time-integrated in situ cosmogenic nuclide production rates using a continuous geomagnetic model, *Earth Planet. Sci. Lett.*, *268*, 190–201, doi:10.1016/j.epsl.2008.01.021.

Matsushi, Y., S. Wakasa, H. Matsuzaki, and Y. Matsukura (2006), Long-term denudation rates of actively uplifting hillcrests in the Boso Peninsula, Japan, estimated from depth profiling of in situ-produced cosmogenic ^{10}Be and ^{26}Al, *Geomorphology*, *82*, 283–294, doi:10.1016/j.geomorph.2006.05.009.

Nishiizumi, K., M. Imamura, M. W. Caffee, J. R. Southon, R. C. Finkel, and J. McAninch (2007), Absolute calibration of ^{10}Be AMS standards, *Nucl. Instrum. Methods Phys. Res., Sect. B*, *258*, 403–413, doi:10.1016/j.nimb.2007.01.297.

Pederson, J. L., K. E. Karlstrom, W. Sharp, and W. McIntosh (2002), Differential incision of the Grand Canyon related to Quaternary faulting—Constraints from U-series and Ar/Ar dating, *Geology*, *30*, 739–742, doi:10.1130/0091-7613(2002)030<0739:DIOTGC>2.0.CO;2.

Pederson, J. L., M. D. Anders, T. M. Rittenhour, W. D. Sharp, J. C. Gosse, and K. E. Karlstrom (2006), Using fill terraces to understand incision rates and evolution of the Colorado River in eastern Grand Canyon, Arizona, *J. Geophys. Res.*, *111*, F02003, doi:10.1029/2004JF000201.

Perg, L. A., R. S. Anderson, and R. C. Finkel (2001), Use of a new ^{10}Be and ^{26}Al inventory method to date marine terraces, Santa Cruz, California, USA, *Geology*, *29*, 879–882, doi:10.1130/0091-7613(2001)029<0879:UOANBA>2.0.CO;2.

Phillips, M. P., E. V. McDonald, S. L. Reneau, and J. Poths (1998), Dating soils and alluvium with cosmogenic ^{21}Ne depth profiles: Case studies from the Pajarito Plateau, New Mexico, USA, *Earth Planet. Sci. Lett.*, *160*, 209–223, doi:10.1016/S0012-821X(98)00076-4.

Polyak, V., C. Hill, and Y. Asmerom (2008), Age and evolution of the Grand Canyon revealed by U-Pb dating of water table-type speleothems, *Science*, *319*, 1377–1380, doi:10.1126/science.1151248.

Reheis, M. C., J. C. Goodmacher, J. W. Harden, L. D. McFadden, T. K. Rockwell, R. R. Shroba, J. M. Sowers, and E. M. Taylor (1995), Quaternary soils and dust deposition in southern Nevada and California, *Geol. Soc. Am. Bull.*, *107*, 1003–1022, doi:10.1130/0016-7606(1995)107<1003:QSADDI>2.3.CO;2.

Repka, J. L., R. S. Anderson, and R. C. Finkel (1997), Cosmogenic dating of fluvial terraces, Fremont River, Utah, *Earth Planet. Sci. Lett.*, *152*, 59–73, doi:10.1016/S0012-821X(97)00149-0.

Riihimaki, C. A., R. S. Anderson, E. B. Safran, D. P. Dethier, R. C. Finkel, and P. R. Bierman (2006), Longevity and progressive abandonment of the Rocky Flats surface, Front Range, Colorado, *Geomorphology*, *78*, 265–278, doi:10.1016/j.geomorph.2006.01.035.

Schaller, M., F. von Blackenburg, A. Veldkamp, L. A. Tebbens, N. Hovius, and P. W. Kubik (2002), A 30,000 yr record of erosion rates from cosmogenic ^{10}Be in middle European river terraces, *Earth Planet. Sci. Lett.*, *204*, 307–320, doi:10.1016/S0012-821X(02)00951-2.

Stone, J. O. (2000), Air pressure and cosmogenic isotope production, *J. Geophys. Res.*, *105*, 23,753–23,759, doi:10.1029/2000JB900181.

Stone, J. O., J. M. Evans, L. K. Fifield, G. L. Allan, and R. G. Cresswell (1998), Cosmogenic chlorine-36 production in calcite by muons, *Geochim. Cosmochim. Acta*, *62*, 433–454, doi:10.1016/S0016-7037(97)00369-4.

Taylor, J. R. (1997), *An Introduction to Error Analysis: The Study of Uncertainties in Physical Measurements*, 2nd ed., 327 pp., Univ. Sci. Books, Mill Valley, Calif.